Materials Science in Semiconductor Processing 154 (2023) 107232

Contents lists available at ScienceDirect

Materials Science in Semiconductor Processing

journal homepage: www.elsevier.com/locate/mssp

Influence of heat treatment on H2S gas sensing features of NiO thin films deposited via thermal evaporation technique

Davoud Dastan [a,1,*], Ke shan [b,1], Azadeh Jafari [c], Tomasz Marszalek [c], Mustafa K.A. Mohammed [d,**], Lin Tao [e,***], Zhicheng Shi [f], Yingxin Chen [g], Xi-Tao Yin [h], Najlaa D. Alharbi [i], Farzan Gity [j], Somayeh Asgary [k], Mohammad Hatamvand [l], Lida Ansari [j]

[a] Department of Materials Science and Engineering, Cornell University, Ithaca, NY, 15850, USA
[b] College of Science, Honghe University, Yunnan Province, 661199, China
[c] Department of Molecular Physics, Faculty of Chemistry, Lodz University of Technology, Zeromskiego 116, 90-924, Lodz, Poland
[d] Radiological Techniques Department, Al-Mustaqbal University College, 51001, Hillah, Babylon, Iraq
[e] School of Chemical Engineering, University of Science and Technology Liaoning, Anshan, 114051, China
[f] School of Materials Science and Engineering, Ocean University of China, Qingdao, 266100, PR China
[g] Institute of Advanced Magnetic Materials and International Research Center for EM Metamaterials, College of Materials & Environmental Engineering, Hangzhou Dianzi University, Hangzhou, 310018, China
[h] School of Physics and Optoelectronic Engineering, Ludong University, Yantai, Shandong Province, 264000, China
[i] Department of Physics, College of Science, University of Jeddah, Jeddah, Saudi Arabia
[j] Micro-Nano Systems Centre, Tyndall National Institute, University College Cork, Cork, Ireland
[k] Department of Physics, West Tehran Branch, Islamic Azad University, Tehran, Iran
[l] Key Laboratory of Flexible Electronics (KLoFE) & Institute of Advanced Materials (IAM), Nanjing Tech University (Nanjing Tech), 30 South Puzhu Road, Nanjing, 211816, Jiangsu, China

ARTICLE INFO

Keywords:
NiO thin Films
Thermal oxidation
XRD
SEM
H_2S detection
Gas sensing

ABSTRACT

In this study, NiO thin films are prepared on Ni foil using thermal evaporation method and the effect of deposition conditions on structural, morphological and H_2S gas sensing properties of NiO thin films is investigated. Structural analysis of the NiO films are conducted by means of X-ray diffraction (XRD), and the films are found to have the FCC phase with preferred (111) and (200) Bragg reflections. Based on XRD and scanning electron microscopy results, it is shown that the crystallite size and the size of homogeneous nanoclusters on the surface of the films increase after increasing oxidation temperature. Also, the EDS patterns of NiO films demonstrate a rise in the intensity of O peak upon increasing the oxidation temperature due to the enhancement of oxygen in the NiO films. The Raman spectrum of NiO thin films several bands correspond to Ni–O vibrations. The obtained gas sensing results demonstrate the sensing response to 20 ppm of hydrogen sulfide at 700 °C. Upon increasing the amount of hydrogen sulfide gas to more than 20 ppm, the fabricated sensors show no significant change in their response, indicating that no additional active sites were exist to interplay with hydrogen sulfide molecules for the higher concentration of hydrogen sulfide. The response of the sensors, recorded 10 s after H_2S gas exposure, depended on the deposition temperature. The current study shows that NiO thin films-based sensors prepared by a simple thermal evaporation method are potentially useful for the detection of H_2S gas.

1. Introduction

Nickel oxide (NiO) is a p type semiconductor [1], semi-transparent material with large direct bandgap between 3.6 and 4.0 eV [2], which make it an interesting candidate for optoelectronic and gas sensing applications [3–6]. There are several deposition techniques to growth NiO thin films via different physical and chemical deposition methods, including Radio Frequency (RF) magnetron sputtering [3,7,8], Direct

* Corresponding author.
** Corresponding author.
*** Corresponding author.
E-mail addresses: d.dastan61@yahoo.com (D. Dastan), mustafa_kareem97@yahoo.com (M.K.A. Mohammed), taolin_phd@163.com (L. Tao).
[1] These authors contributed equally.

https://doi.org/10.1016/j.mssp.2022.107232
Received 8 July 2022; Received in revised form 12 November 2022; Accepted 16 November 2022

Current (DC) magnetron sputtering [6], pulsed laser deposition (PLD) [9], chemical bath deposition [10], chemical vapor deposition [11], vacuum evaporation [12], sol–gel process [13–15], thermal evaporation [16], ion beam sputtering [17], spin coating [18], and electron-beam evaporation [19]. Because of its interesting properties such as high electrochromic efficiency, large dynamic range, good cyclic reversibility, and low material cost, the NiO is a promising material for many different applications.

Semiconductor oxides has numerous advantages due to their properties tenability for seversal applications [20–31]. Among them, NiO has numerous potential applications such as magneto-electronic devices [2], electro chromic display [3], super capacitors [4,20,24], resistive switching [9], and IR window [10] due to its semiconducting, semi-transparent, catalytic, excellent electrical, and thermoelectric properties. In addition, nickel oxide in different crystal structures (such as thin film, nanoparticles, nanowire among others) have been studied as an attractive material for gas sensing and have shown propitious sensing features after exposing to different gases including CO, NO_2, H_2, and NH_3 [32–35]. Due to its wide band gap and excellent electrical properties, recently nickel oxide has been used for the detection of H_2S gas as a poisonous, corrosive, and flammable gas [36]. Previous report demonstrated that the optimum temperature to obtain a sensitivity of 94% is 150 °C for the NiO films [36]. C. Luyo et al. fabricated nano-crystalline NiO gas sensors using advanced reactive gas deposition and demonstrated the NiO can detect H_2S and NO_2 gases at ambient condition and the best acting temperature for achieving the highest sensitivity was from 150 to 162 °C [37]. As another example by S. K. Ganapathi et al. NiO NPs were prepared by a simple and cheap chemical coprecipitation route and the gas-sensing characteristics showed good sensitivity to H_2S gas [38]. Among techniques used to deposit NiO thin films, thermal evaporation of Ni foil is a low cost and simple method to prepare high purity NiO films [39,40].

In this study, we report growth of NiO thin film with oxidation Ni foil at different oxidation temperatures. Thermal evaporation is considered as a facile method to prepare different metal oxide films on rigid substrate. This technique possesses multiple merits against other chemical methods including easy processing and mass production of nanostructured metal oxides in absence of dangerous chemicals [41]. We further investigated the influence of various oxidation temperatures on the structural and H_2S sensing features of NiO thin films. There are limited studies on the gas-sensing behavior of NiO and the interaction of H_2S with NiO. Herein, the characterization of NiO thin films as gas sensing material was accomplished against H_2S and a correlation between nanostructure and sensing properties of NiO thin films is discussed in details.

2. Experimental section

2.1. Fabrication of gas sensors using NiO thin films

Initially, the platinum (Pt) electrodes were prepared using a shadow mask by electron beam evaporator method before deposition of NiO thin films as the sensing materials on alumina substrates. Then, the Pt electrodes were annealed at 700 °C for 4 h. A second mask was fixed on the substrates which were located into a horizontal quartz tube for the oxidation in the air. Using thermal evaporation method, nickel oxide thin films were prepared in a horizontal quartz tube. Nickel foils (0.15 mm thick and 99.999% purity) were cut into1cm × 1 cm pieces and used. The deposition temperature and the process of film growth were controlled by a thermocouple placed near the Ni foil. The black thin layers of NiO were formed on the substrates surfaces at different deposition temperatures 500, 600, 700, and 800 °C for 240 min duration (see Fig. 1 (e)). It should be noted that oxidation time is constant in all four conditions. It was found that at temperature $T \leq 900$ K the oxidation of is a self-stabilizing process.

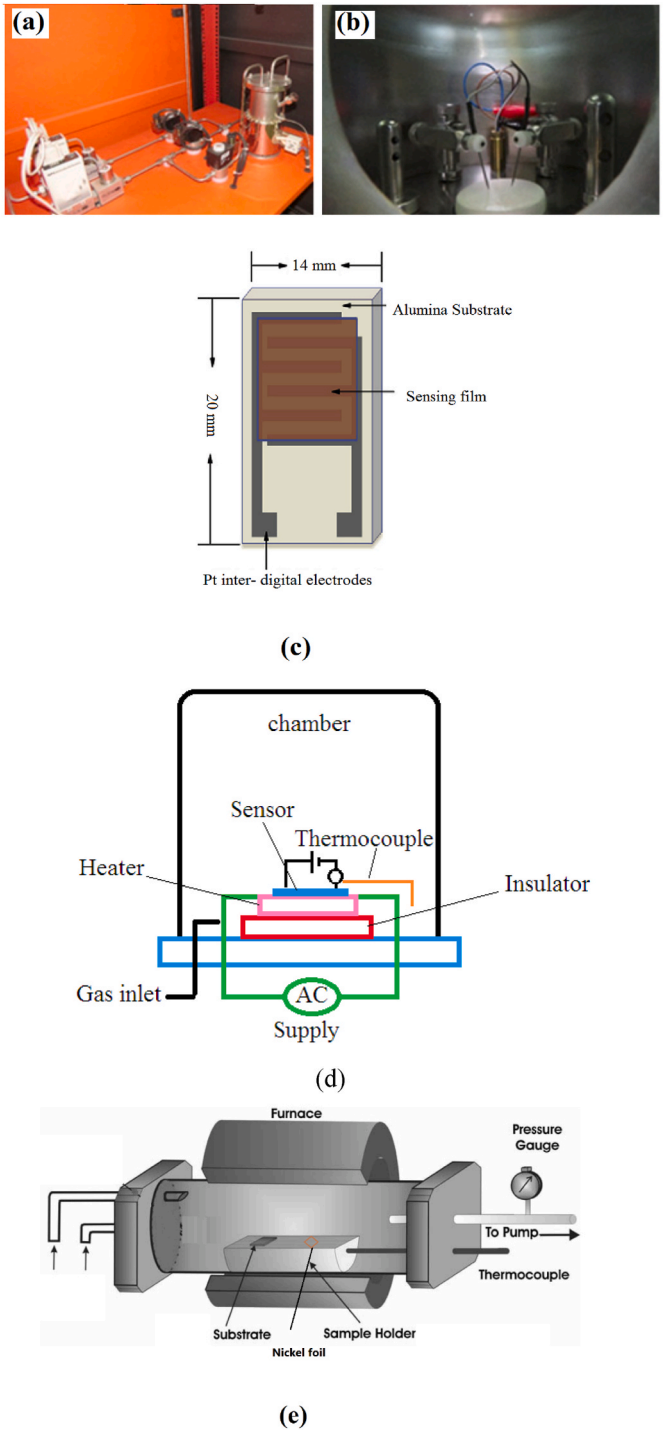

Fig. 1. (a) and (b) Gas sensing system, and (c) and (d) the schematic representation of the sensor structure and gas sensing system and (e) horizontal quartz tube.

2.2. Evaluation of gas sensing performance

Fig. 1 demonstrates static gas sensing system which was used to evaluate. The sensing performance of the films. The test chamber is made of cylindrical stainless steel with a diameter of 30 cm and a height of 30 cm with viewing glass windows to view the testing process. The system is also equipped with a ceramic convection heater. It can also be programmed in stages (CYCLIC) from ambient temperature up to 500 °C to adjust the surface temperature of the gas sensor during testing. The system is equipped with a two-stage rotary oil vacuum pump to create

vacuum in the chamber. The system is equipped with two gas inlet channels and two gas mass flow controllers (MFC) to control the gas flow and concentration with a high accuracy. It is also possible to add moisture to the gases as well as step-by-step programming (CYCLIC) to the MFCs in terms of flow rate per unit time. The system has a temperature and humidity sensor in the testing chamber to monitor and control the temperature and humidity during the testing process. The system is equipped with stainless steel solenoid valves to control the concentration process manually. It is also equipped with automatic process control system, programmable logic controller (PLC) and a touch screen to fully control the testing process. All changes in temperature, pressure, humidity, and gas flow are recorded as data in Excel software. The system has an accurate dual-channel multimeter to read the changes of the gas sensor output (resistance, conductivity, and I–V changes). There is also dedicated software for reading the output with full features required for testing. From I–V characteristics, the change in resistance was noted. The change in current was recorded upon applying a constant voltage to the sensors while they were exposed to H_2S gas. The sensor response is described as amount of conductance variation for the tested gas to the conductance in the air. Thus, the sensitivity of the sensors is estimated using equation (1):

$$S = \frac{R_a - R_g}{R_a} \tag{1}$$

where R_g is the sensor resistance in existence of the tested gas and R_a is the sensor resistance in dry air. Additionally, the sensing response of sensors (R) at a constant operating temperature is considered as follow [39–41]:

$$R = \frac{R_a}{R_g} = 1 + kC^n \tag{2}$$

where, '*C*' is the content of the target gas, and the response is denoted by the prefactor 'k', and exponent 'n'. The response time is defined as the amount of time that a sensor requires to achieve 90% of the maximum variation in resistance upon exposure to the target gas and the amount of time that a sensor requires to get back to 90% of the initial resistance is called as the recovery time. These two important parameters are extracted from the graph of change in sensitivity against time (see our previous works [39,40]).

2.3. Characterization techniques

X-ray diffraction (STOE–XRD diffractometer) with Cu Kα radiation wavelength (λ) of 1.54060 Å was used to identify the structural properties of the samples. The morphology of the samples was investigated using top view field emission scanning electron microscopy (FESEM, Leo 440i). The elemental composition of NiO films was accomplished via energy dispersive X-ray (EDX) spectroscopy. Raman spectroscopy (Thermo Nicolet-Raman 960) with a helium neon (He, Ne) laser of 633 nm wavelength, power Output: 17 mW without Plasma Line Rejection Filter was used to further corroborate the phase formation of the NiO samples.

3. Results and discussion

3.1. XRD analysis

XRD characterization can give information about the crystallinity and crystallite size. The crystal structure of NiO thin films was determined by using X-ray diffractometer. Fig. 2 delineates the XRD patterns of the NiO samples fabricated at various thermal evaporation temperatures. The diffraction peaks in the XRD patterns at $2\theta = 37.25°$ and 43.30° correspond to the (111) and (200) planes of the FCC phase of NiO (JCPDS No. 04–0835). In addition, the peak at $2\theta = 51.3°$ is related to the FCC phase of Ni. The average crystallite size (D) is calculated using

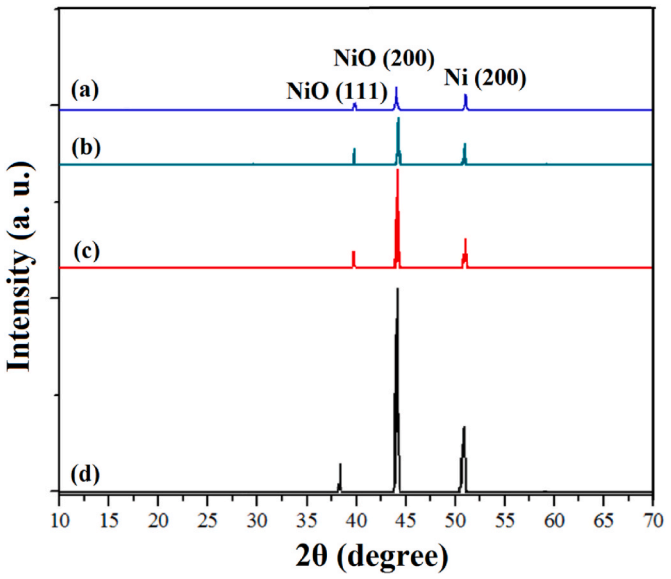

Fig. 2. XRD patterns of samples at different oxidation temperatures (a) 500, (b) 600, (c) 700, and (d) 800 °C.

the Scherrer equation [42–45]:

$$D = 0.9\lambda / \beta \cos\theta \tag{3}$$

where, β is the half width of diffraction peak measured in radians. The NiO film thickness is evaluated by Detak3 surface profilometer and the results are presented in Table 1. It is clear that as the thickness increases, the XRD peaks intensity increase. The position of XRD peaks are impacted by the size of particle and their FWHM is reversibly related to crystallite size. The area of peaks represents integral intensity in the XRD analysis and their FWHM reduce when the crystallite size increases which results in a proportional growth to keep their areas constant. It is worth noting that the growth orientation of crystals influences the XRD peaks intensity. In the current research, the intensity of (200) peak is much higher than the other directions and the crystallites are oriented mainly along the (200) direction. From the XRD patterns, it is observed that all the films are polycrystalline, and the intensity of the (200) diffraction peak was observed higher compared with other peaks indicating the preferred orientation. Preferred orientation arises when there is a stronger tendency for the crystallites in a powder or a texture to be oriented more one way, or one set of ways, than all others. Since, the intensity of the X-ray diffraction line depends on the elemental composition of the sample and its preparation conditions, during the thermal evaporation process, the crystallites may take a certain direction for their growing and samples may have a preferred orientation for their growth.

Other development by Chen et al. showed that the thickness of the films has a vital role in crystallinity [2] and the crystallinity of the NiO film can be tuned upon raising the films thickness. As the oxidation temperature increases, the agglomeration of oxide scales increases therefore, the crystallite size increases (see Table 1). Also, as can be seen from Fig. 2, when the temperature gradually raises, the intensity of NiO

Table 1
Crystallite size of samples at various oxidation temperatures of 500, 600, 700, and 800 °C for 240 min duration.

Sample number	Thermal evaporation temperature (°C)	Crystallite size (nm)	Film thickness (nm)
(a)	500	31	120
(b)	600	38	156
(c)	700	52	180
(d)	800	73	210

(200) peak increases.

The reason for this change in XRD patterns is that when temperature increases in the oxidation process, the Ni atoms at higher temperature have enough thermal energy to reach the Ni foil and form a mainly (200) crystallite orientation in NiO structure. It can be concluded from peak intensity in XRD pattern that NiO films grow preferentially along the (200) direction because the intensity of (200) is more than (111). It is evident from Table 1 and using equation (3), that the sample prepared at 800 °C presents the highest value of crystallite size (73 nm) which confirms the development of nanostructure NiO sample. This enhancement of the grain size stemmed from a decrease in the lattice defects, which cases reduction of internal strain and dislocation density [39]. Moreover, it is reported that during the formation of NiO thin film, the oxygen solubility of the nickel matrix increases as the oxidation temperature increases [40].

Ni oxidation in oxygen atmosphere is composed of three steps at high temperature: a diffusion of the oxygen gas, a diffusion of the oxidizing species, and the reaction of these species with the nickel atoms. Notably, upon increasing temperature to 800 °C, the intensity of the NiO (200) peaks increases implying the development of NiO crystals and the improvement of Ni–O bonding to form a thin oxide layer on the Ni surface. This concept was previously confirmed by Valladares et al. for the thermal evaporation of Ni thin films prepared vis traditional thermal evaporation process [46]. The results showed that the oxidation and structure of NiO thin films depends on thermal evaporation temperature. In other words, the oxidation nature of Ni thin films depends on the temperature. As another example, Pinnel et al. stated that the oxidation of Ni begins slowly due to the exposure to oxygen atmosphere [47]. A similar result was reported on thermally oxidizing an evaporated Ni thin film at 500 °C and the effect of temperature was investigated systematically [48].

3.2. SEM analysis

Fig. 3a–d illustrates SEM images at 500 nm scale of NiO films prepared at different oxidation temperature (500, 600, 700, and 800 °C) for detail information about size, shape and mechanism of the grain growth. The SEM morphologies of almost all films appear to have spherical grains throughout their entire surface. It can be seen from Fig. 3 that the surface topography in all samples was nanoclusters without cracks and pinholes with random distribution of grain sizes and shapes. The polydispersity behavior of the grain size are possibly owing to the rate of particle growth and their incomplete nucleation. It has been reported that grain formation on the surface of metallic foils as a starting material in thermal evaporation process has been related to effective factors in growth mechanisms such as vapor-solid, solid-liquid-solid, diffusion limitations, and stress mechanisms [49,50]. Several morphologies have been observed in previous research related to NiO thin film such as nano-sheets [39], nano-wires [40], nano-fibres [41], cactus like nano-structure [42], hemisphere [43], nano-flowers [44]. The overgrown clusters in the smaller grains of NiO thin film prepared by spray method on glass and FTO substrate has been reported [51] and the results showed that the deposition parameters of NiO film have an effect on the surface texture and grain size of the film.

Also, thermal evaporation has been employed to prepare nanocrystalline NiO thin films on Ni foil with regular and small grains and the results showed that increase of annealing temperature caused to agglomeration of grains and hence enhancement of particles sizes [34–36]. In our work, the SEM micrographs demonstrate that the morphology largely depends on the oxidation temperature. Generally, parameters including O_2 pressure, temperature of oxidation process, heating environment and the heat duration impact on the kinetics of oxidation reaction in metal oxide thin films. Moreover, the process of Ni oxidation occurs slowly right after the film deposition because Ni gets exposed to the air (Fig. 3). This process happens owing to two reasons: (i) transfer of electrons at the interface to develop a monolayer of an adsorbed oxygen ion at the surface and (ii) diffusion of oxygen anion into the metal film [39]. Initially, the oxygen anions occur to create a thin layer of oxide film on the surface of the nickel. The surface of nickel gets oxidized quickly to develop nickel oxide thin films. Moreover, the surface of nanostructured NiO contains the grains with clear boundaries distributed on the surface of the films which act as sensing material or an active area for the gas detection. The Ni atoms reoccupy to the preferred sites and interlay with the air in the first calcination step. The nucleation sites are mainly structural defects and available on the surface for nickel oxide and they have a lateral growth. The origin of these defects could be

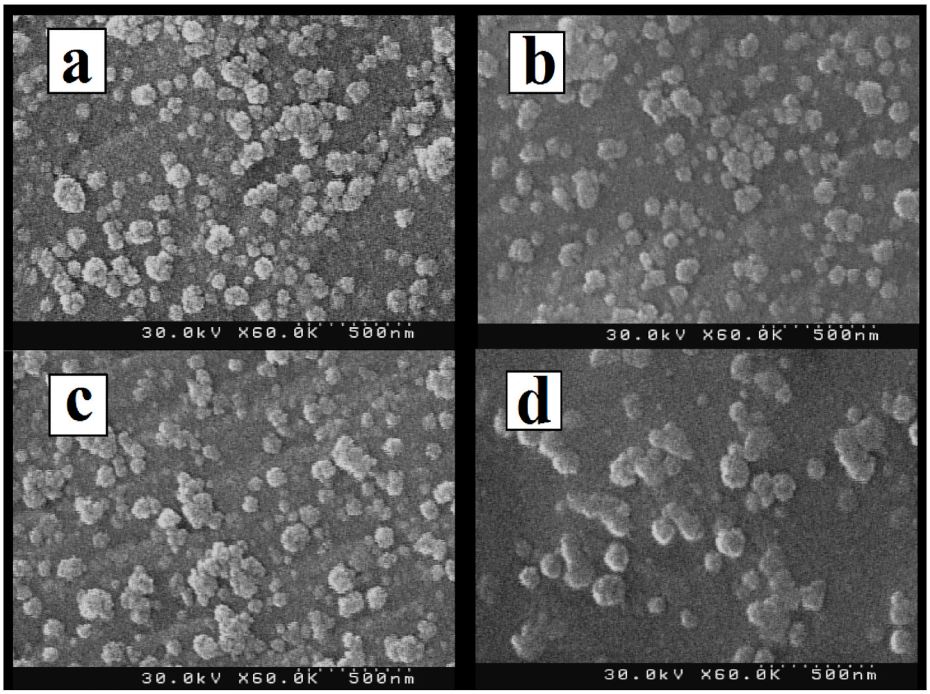

Fig. 3. SEM images of samples at various oxidation temperatures (a) 500, (b) 600, (c) 700, and (d) 800 °C.

dislocations, dust particles, grain boundaries, and other impurities [52–54].

It seems that an increase in the oxidation temperature leads to a rise in the number of nucleation sites and atoms, therefore molecules on the Ni surface can move and react with each other and as a result, seeds and nuclei formed on the surface and agglomeration of grains occurred. At higher oxidation temperature, there was stronger interaction between Ni substrate and O_2 as ad-atoms. The high mobility of ad-atoms results in film with larger crystallites on the surface. With increasing oxidation temperature, the crystal quality of the films improved which is in a good agreement with XRD spectrum. Additionally, the size of nano-dots from SEM images are less than 100 nm, which are correlated with the calculated average crystallite size from XRD (see Table 1). Higher oxidation temperature leads to larger surface mobility and diffusion length of oxygen atoms on the Ni surface which improves the crystal quality [55].

3.3. EDS analysis

EDS technique was used to identify the elemental composition of NiO thin films. In Fig. 4, the EDS results of NiO films prepared at different oxidation temperatures are demonstrated. As can be seen from Fig. 4, only Ni and O elements are present in all the EDS patterns. Since the area covered by an EDS peak is directly proportional to the abundance of specific element in the sample, it can be seen that by increasing the temperature the intensity of O peak increases which is related to enhancement of oxygen in the NiO films. For oxidation temperatures 500, 600, 700, and 800 °C the peak intensities are 670, 980, 900, and 1650 respectively, therefore maximum amount of oxygen with the highest peak intensity is observed at 800 °C.

3.4. Raman analysis

Vibrational property of NiO thin films has been studied by Raman study. Raman analysis was used to determine the molecular vibrations and the chemical structure and confirm the nature of inorganic compounds. Also, the phonon Raman scattering has been used to recognize the defect activated details. The Raman spectrum of nickel oxide thin films (Fig. 5) shows several bands that correspond to Ni–O vibrations. The Raman scattering in nickel oxide originates from one-phonon, two-phonon excitations as well as one-, two-, and four-magnon excitations. NiO is an antiferromagnetic material; it has two types of magnons associated with the spin of electrons in two types of atoms; one with spins up and the other with spins down. The nature of magnons depends

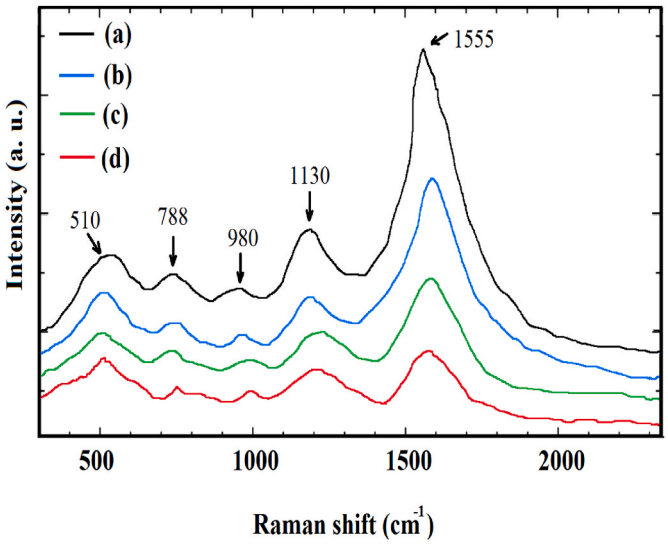

Fig. 5. Raman spectra of samples at various oxidation temperatures (a) 500, (b) 600, (c) 700, and (d) 800 °C.

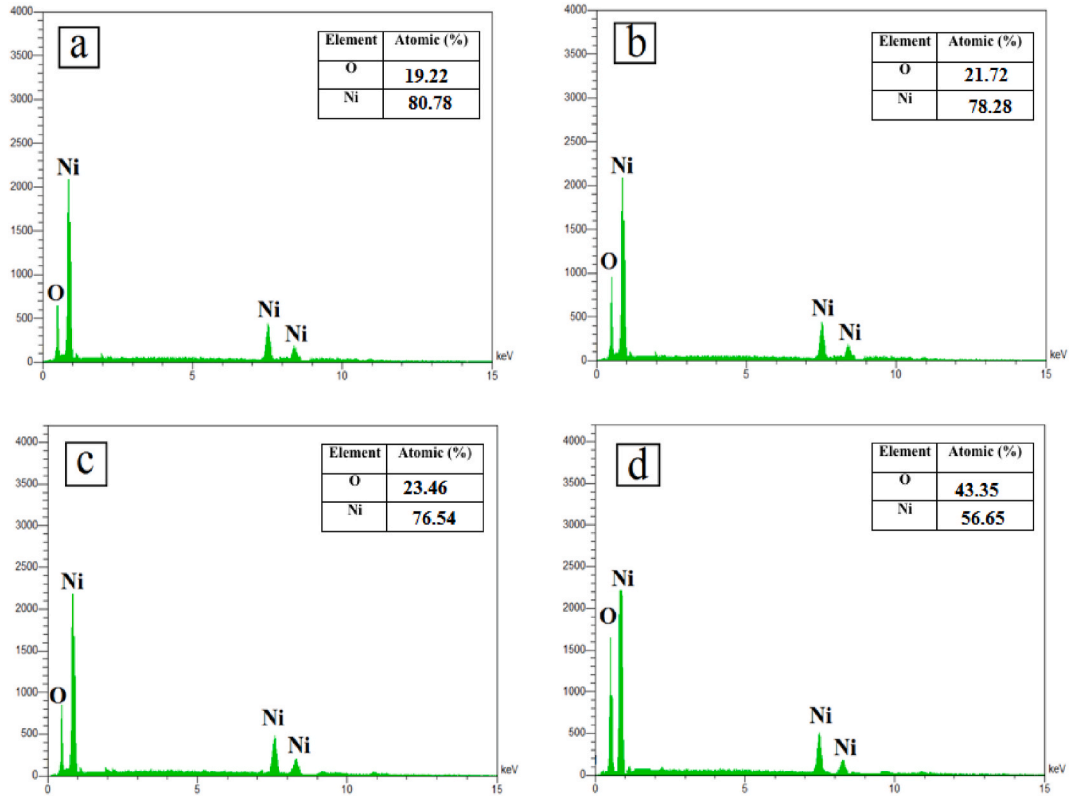

Fig. 4. EDS analyses of samples at various oxidation temperatures (a) 500, (b) 600, (c) 700, and (d) 800 °C.

on the structure of NiO at ground state [57]. The bands have been identified as one-phonon scattering (transverse optical (TO) phonon mode at 510 cm^{-1}), two-phonon scattering (2TO at 788 cm^{-1}, TO + LO (longitudinal optical) at 980 cm^{-1} and 2LO at 1130 cm^{-1} [56–59]). The appearance of LO phonon could be due to Ni vacancy defects. The strongest band at ~1555 cm^{-1} corresponds to two-magnon excitations (2 M). All Raman active modes in NiO have the same frequency in relation to the LO mode because NiO crystallizes in a cubic form, which causes it to have its isotropy features. Also, the phonon scattering is due to the presence of lattice defects, that lower the symmetry around the atoms normally participating in the formation of phonons in a perfect single crystal; and the non-stoichiometry in the composition of oxygen is considered to be the major reason behind this phenomenon [59]. Appearance of the first-order phonon peak (1P) could correlate with crystal imperfections (or distortion) and its intensity is related to the quality of the films (by normalization of the first-order Raman peak (I_{1P}) intensity to one of the second-order peaks (I_{2P})). The second-order Raman scattering (2p) in Raman spectra could correlate with perfect crystals [60]. It was suggested by Jiang et al. [61] and Wruck et al. [62] that the first-order LO phonon scattering in NiO indicating the presence the Ni vacancy defects or Ni^{3+} ions. The influence of different oxidation temperatures on nickel oxide thin films was detected by the changes in Raman modes intensity. The intensity of all Raman scattering modes has dramatic decrease with increasing oxidation temperature. Reduction of the first-order Raman peak (1P) intensity represents better crystal quality of NiO thin films with increasing oxidation temperature that showed by XRD results [63].

We can see that the 2P peaks have red-shift (shift to lower frequencies). It was ascribed by biaxial strain in the thin NiO films [59]. The 2 M Raman band showed significant broadening and reduction of intensity with a little shift to lower energy. Similar behavior was reported by Mironova-Ulmane et al. [64]. They reported that the 2 M peak intensity decreased with increasing particle size and showed a little shift to lower frequency and broadened. Also, Kumar et al. [65] found that with increasing annealing temperature, the 2 M Raman intensity decreased. Crystalline rearrangement can explain this affect and it is responsible for describing the preferential directions. The 2 M bands in crystalline NiO phase reveal relatively strong antiferromagnetic ordering. The broadening effect in 2 M bands can be related to decrease of antiferromagnetic spin correlations that are responsible for the transition of antiferromagnetic-to-paramagnetic in nanosized NiO [66].

3.5. Sensing properties

Based on the change in the conductivity or electrical resistance of thin film, the mechanism of gas sensing of NiO thin film is evaluated. The values of current are recorded after applying a constant voltage to the sensors based on NiO thin film under hydrogen sulfide exposure. The actual process of sensing evaluation goes like this: first, the air is passed through the chamber for 10 min. Next, the target gas is introduced in the system, and the variation in the resistance of sensor is recorded for the next interval of 10 min. Lastly, the target gas flow is stopped and only the air is passed through the chamber to clean it. Dynamic response curves of NiO thin film sensors at different H_2S concentrations has been shown in Fig. 6. As expected, the value of sensor resistance is not constant while the target gas is exposed to the surface of the sensing materials. The aforementioned cycle can be repeated and the variation in the resistance of the sensing materials can be recorded for a long period of time.

In this way, the sensing of the sensor is recorded and compared to the reported values for the similar sensors based on NiO NPs [66–68]. The gas sensing response of the fabricated nickel oxide sensors to various concentration of hydrogen sulfide at elevated operating temperatures is demonstrated in Fig. 7. After exposing the surface of sensor to the target gas, adsorption and desorption phenomena happen on the surface of the sensor and at the interface between the sensing materials and the gas

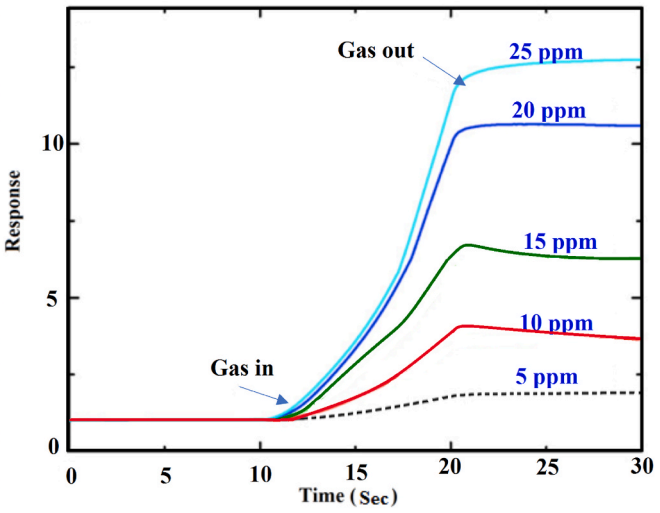

Fig. 6. Dynamic response curves for various H_2S concentrations for NiO thin film gas sensor. Data were taken at room temperature.

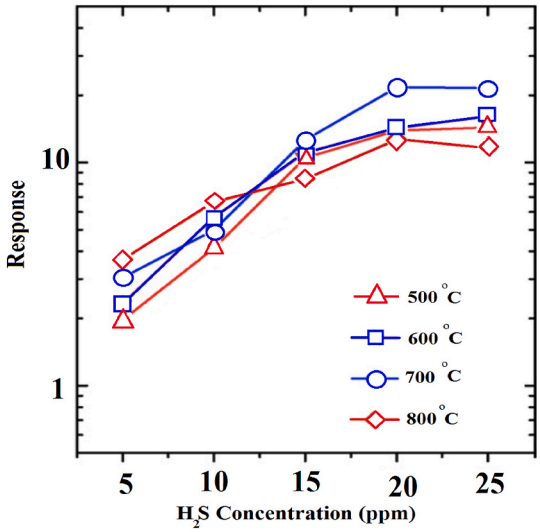

Fig. 7. Sensor response vs. H_2S concentration for NiO thin film gas sensors samples at various oxidation temperatures: 500, 600, 700, and 800 °C.

molecules, and as a result, the electrical resistivity of the sensing materials become constant for the equal values of the absorption and desorption of the exposed gas.

Upon exposing the NiO based sensor to hydrogen sulfide, an increase in the resistance of the sensor is recorded due to the fact the NiO is a p-type material and interactions between its molecules and hydrogen sulfide molecules lead to an adsorption of O_2 molecules on the grains surface. In a typical p-type material including copper oxide and nickel oxide, negative charges are majority and electrons migrate from valence band to oxygen molecules which are adsorbed on the surface and result in the existence of a hole-accumulation layer at the grain boundaries [67,68]. It is well known that an n-type semiconductor has electrons as a major charge carrier and p-type semiconductor has holes as a major charge carrier. NiO is a p-type semiconductor, and the charge carriers are positive holes. And, the adsorption and desorption of the H_2S on the surface of the NiO will result in the changes of electrical resistance. However, the sensor performance of NiO depends on the number of free electrons in the outermost shells, which is greatly influenced by the change in resistance of the sensor. NiO has a 3 d^8 electronic

configuration, and its triply degenerate state (t_{2g}) is filled with one free electron in a doubly degenerate (e_g) state; these free electrons facilitate the electron transport mechanism. It can be seen from Fig. 7, the sensor prepared at 700 °C shows the best performance due to more active areas which can be seen from SEM image in Fig. 3 (c).

Although the gas sensing response to hydrogen sulfide is more complex in Fig. 8. It is seen that the NiO sensing response increases for a low level of hydrogen sulfide content after raising the oxidation temperature. This phenomenon is less likely attributed to the raise in grain size, because the growth of grains is negligible till 700 °C. It is very likely that the interplays between nickel oxide and hydrogen sulfide is most likely low at ambient condition. It is believed that the nickel oxide nanoparticles possess enough reaction sites to generate a series of complete reaction, hence causing a rise in the sensor response for low amount of hydrogen sulfide gas as demonstrated in Fig. 7. It is evident that as the amount of hydrogen sulfide increased above 10 ppm, the sensor response experiences an improvement up to 700 °C.

Although, a reduction in the sensor response is observed at oxidation temperatures of 800 °C for the same level of hydrogen sulfide. Such behavior is expected due to a reduction in the surface to volume ratio at oxidation temperature of 800 °C because of the augmentation in the grain size. In addition, a saturation in the sensing response of the sensors is pronounced upon further increasing the amount of hydrogen sulfide as delineated in Fig. 7, suggesting lack of additional active sites on the surface of the sensor to interplay with new hydrogen sulfide molecules when the amount of target gas increases. As the oxidation temperature increases the grain sizes of NiO thin films increase which are also consistent with the obtained results of the FESEM images and the XRD analyses.

The concept of oxidation reaction and its impact on the sensing performance of the sensors based on NiO as sensing material exposed to hydrogen sulfide is important to be discussed. The level of interplays between the molecules of sensing materials and the molecules of the target gas is a function of the oxidation temperature and the size of the sensing materials grains. The sensing response of gas sensors based on semiconductor oxides and the sensors resistivity in impacted by the grain boundary potential barrier height at nano level, hence, gas sensing phenomenon is a surface-dependent event. When NiO is subjected to hydrogen sulfide, two primary reactions occur. The first is the oxidation

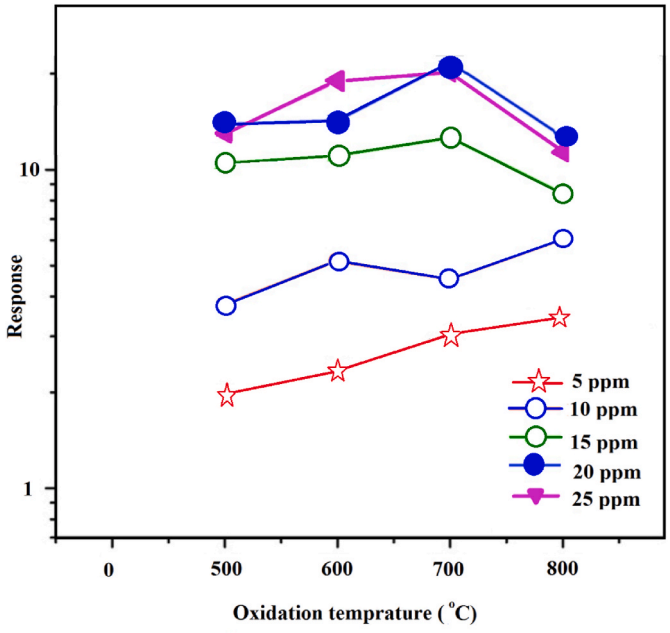

Fig. 8. Sensor response vs. oxidation temperature for NiO thin film gas sensors at the shown H_2 S concentrations.

of hydrogen sulfide with oxygen molecules that have been adsorbed and in turn result in an improvement in the resistance of NiO sensing materials). Second, NiS formation as a result of the interactions between hydrogen sulfide molecules and nickel oxide molecules, that in turn lead to a decrease in the sensor resistance owing to the metallic nature of NiS.

As an alternative to the advanced tools, the chemiresistive metal oxide-based semiconductor sensors offer advantages for H_2S detection at low ppm level. Industrially accepted short-term and long-term threshold limit values for H_2S gas are reported to be 10 and 15 ppm, respectively. Although, it can be easily detected by its characteristic rotten-egg smell, at relatively higher concentrations, H_2S paralyzes the olfactory system, making it essential to monitor its presence. Fe_2O_3-loaded NiO nanoplates were reported to exhibit high response and excellent selectivity toward H_2S. Au@NiO yolk−shell NPs prepared by Rai et al. showed a higher response of 108.92 at 300 °C for 5 ppm of H_2S [69–71]. It has been reported the response of H2S gas sensors using low level gas:

Poongodi et al. fabricated a tungsten oxide nanostructured thin film by the electro-deposition method for hydrogen sulfide gas sensing at low concentrations, ranging from 0.1 to 10 ppm. The resistance of the sensor decreased upon exposure to each H_2S pulse and recovered completely to the initial value upon stopping the supply of H_2S gas and exposure to air due to the reversible reaction of the film component with the gas molecules [72]. The similar sensing behavior of increasing conductivity at the metal oxide film surface was observed with pure n-type barium titanate which gave a maximum response to hydrogen sulfide gas at an optimum temperature of 350 °C [73]. Tin oxide film resulted in a 48% response for 5 ppm H_2S at 300 °C [73], thus indicating the high dependency of sensitivity on operating temperatures.

Joshi et al. [74] prepared a polycarbazole (PCz) film-based chemiresistor by the Langmuir–Blodgett technique on flexible bi-axially oriented polyethylene terephthalate substrate. They obtained very stable 11, 35 and 71 Langmuir multilayer (ML) films with liquid expanded character. Among the deposited films, only 35 and 71 ML films were responsive as a typical p-type semiconductor to H_2S at 10 ppm, which may be attributed to the absence of enough active sites for gas reactions on the surface of 11 ML film [75]. Liu et al. [76] developed a PANI nanofibers-based film using the electrochemical method. The film had no response to sample gas, while gold nanoparticles incorporating PANI nanofiber showed an 80% maximum response towards 1 ppm H_2S gas. These are just a few examples where low-level of H_2S detection is reported by other researchers.

4. Conclusion

Using thermal evaporation method, NiO thin films were synthesized on Ni foil and the effect of thermal evaporation from 500 to 800 °C on structural, morphological and H_2S sensing property of the NiO thin film was investigated. The structural analyses from XRD patterns of the films indicate that they are polycrystalline and have a FCC structure. The SEM micrographs indicate that the morphology is highly sensitive to oxidation temperature and by increasing oxidation temperature, the drain size and crystal quality of the films improved. The obtained EDS spectra approve the existence of nickel and oxygen elements in the film. Also, the Raman spectrum shows several bands corresponds to Ni–O vibrations. Gas sensing properties showed that at lower H_2S concentrations (5 and 10 ppm), the gas response increases with increasing oxidation temperature. In addition, the sensor response of the NiO thin film which prepared on 700 °C oxidation temperature against 20 ppm H_2S is more than other samples and showed excellent response which may be related to grain size and well-crystallized structure. Comparing the present results with those in the literature [7–15], it stands out clearly that NiO thin film can be considered an excellent candidate for fabricating highly sensitive and selective H_2S chemical gas sensors. This study demonstrates that NiO thin films-based sensors prepared by a simple thermal evaporationtechnique are potentially useful for the detection of H_2S gas.

CRediT authorship contribution statement

Davoud Dastan: Conceptualization, Writing – original draft, Data curation, Formal analysis, Supervision. **Ke shan:** Conceptualization, Methodology, Writing – review & editing. **Azadeh Jafari:** Investigation, Resources, Software. **Tomasz Marszalek:** Investigation, Resources. **Mustafa K.A. Mohammed:** Formal analysis, Software. **Lin Tao:** Writing – review & editing. **Zhicheng Shi:** Investigation, Resources. **Yingxin Chen:** Investigation, Resources. **Xi-Tao Yin:** Software, Validation. **Najlaa D. Alharbi:** Resources. **Farzan Gity:** Writing – review & editing, Investigation. **Somayeh Asgary:** Resources. **Mohammad Hatamvand:** Software, Resources. **Lida Ansari:** Writing – review & editing.

Declaration of competing interest

The authors declare that they have no known competing financial interests or personal relationships that could have appeared to influence the work reported in this paper.

Data availability

No data was used for the research described in the article.

Acknowledgment

Azadeh Jafari and Tomasz Marszalek acknowledge the Foundation for Polish Science financed by the European Union under the European Regional Development Fund (POIR.04.04.00-00-3ED8/17).

References

[1] M.A. Wittenhaur, L.L. Van Zandt, Philos. Mag. B 46 (1982) 659.
[2] H.L. Chen, Y.N. Lu, W.S. Hwang, Thin Solid Films 498 (2006) 266.
[3] P. Horak, V. Lavrentiev, V. Bejsovec, et al., Eur. Phys. J. B 86 (2013) 470.
[4] Ke Shan, Zhong-Zhou Yi, Xi-Tao Yin, Davoud Dastan, Hamid Garmestani, Dalton Trans. 49 (2020) 8549–8556.
[5] S. Mohammad Beigia, F. Mesgari, M. Hossein, D. Dastan, G. Xu, Curr. Anal. Chem. 18 (2022) 53–62.
[6] V. Gowthami, P. Perumal, R. Sivakumar, C. Sanjeeviraja, Phys. B Condens. Matter 452 (2014) 1.
[7] J.P.B. Silva, K.C. Sekhar, R.F. Negrea, C. Ghica, D. Dastan, M.J.M. Gomes, Ceram. Int. 48 (2022) 6131–6137.
[8] D. Dastan, K. Shan, A. Jafari, F. Gity, X. Yin, Z. Shi, N. Alharbi, B. Reshi, W. Fu, Ş. Ţălu, L. Aljerf, H. Garmestani, L. Ansari, Appl. Phys. 128 (2022) 400.
[9] N. Duraisamy, A. Numan, K. Ramesh, et al., Mater. Lett. 161 (2015) 694.
[10] I. Porqueras, E. Bertran, Thin Solid Films 398 (2001) 41.
[11] V. Gowthami, M. Meenakshi, P. Perumal, P. Sivakuma, C. Sanjeeviraja, Mater. Sci. Semicond. Process. 27 (2014) 1042.
[12] M.L. Grilli, I.D. Sarcina, S. Bossi, A. Rinaldi, Pilloni L and Piegari A, Thin Solid Films 594 (2015) 261.
[13] M.F. Al-Kuhaili, S.H.A. Ahmad, S.M.A. Durrani S M A, et al., Mater. Sci. Semicond. Process. 39 (2015) 84.
[14] A. Timoumi, D. Dastan, B. Jamoussi, K. Essalah, O. Alsalmi, N. Bouguila, H. Abassi, R. Chakroun, Z. Shi, Ş. Ţălu, Mol. 27 (2022) 6151.
[15] X. Yin, H. Huang, J. Xie, D. Dastan, J. Li, Y. Liu, X. Tan, X. Gao, W. Shah, X. Ma, Green Chem. Lett. Rev. 15 (3) (2022) 546–556.
[16] I. Sta, M. Jlassi, M. Kandyla, et al., Int. J. Hydrogen Energy 41 (2016) 3291.
[17] R.K. Jamal, K.A. Aadim, Q.G. Al-Zaidi, I.N. Taaban, Photonic Sens 5 (2015) 235.
[18] E.S. Hassan, A.A. Saeed, A.K. Elttayef, J. Mater. Sci. Mater. Electron. 27 (2016) 1270.
[19] Z. Liu, T.P. Chen, Y. Liu, S. Zhang, Int. J. Appl. Ceram. Technol. 10 (2013) 20.
[20] P. Zhu, D. Dastan, L. Liu, L. Wu, Z. Shi, Q. Chu, F. Altaf, M. Mohammed, J. Mol. Graph. Model., 118 (2023) 108335.
[21] I. Ashraf, S. Ahmad, D. Dastan, C. Wang, H. Garmestani, M. Iqbal, Electrochim. Acta 429 (2022), 141036.
[22] I. Ashraf, S. Ahmad, F. Nazir, D. Dastan, Z. Shi, H. Garmestani, M. Iqbal, Int. J. hydrog. energy 47 (2022) 27383–27396.
[23] L. Liang, Z. Shi, X. Tan, S. Sun, M. Chen, D. Dastan, B. Dong, L. Cao, Adv. Mater. Interfac. (2022), 2101646.
[24] Moses J. Kartha, Bilal Ahmad Reshi, Pravin S. Walke, Davoud Dastan, Ceram. Int. 48 (2022) 5066–5074.
[25] S. Xia, Z. Shi, L. Sun, S. Sun, D. Dastan, R. Fan, Mater. Lett. 312 (2022), 131654.
[26] L. Sun, Z. Shi, B. He, H. Wang, S. Liu, M. Huang, J. Shi, D. Dastan, H. Wang, Adv. Funct. Mater. 2021, 2100280.
[27] M. Zhang, Z. Shi, J. Zhang, K. Zhang, L. Lei, D. Dastan, B. Dong, J. Mater. Chem. C 9 (2021), 10414.
[28] M. Han, Z. Shi, W. Zhang, K. Zhang, H. Wang, D. Dastan, R. Fan, Compos: Part A 149 (2021), 106559.
[29] M. Asadzadeh, F. Tajabadi, D. Dastan, P. Sangpour, Z. Shi, N. Taghavinia, Ceram. Int. 47 (2021) 5487–5494.
[30] S. Wei, Z. Shi, W. Wei, H. Wang, D. Dastan, M. Huang, J. Shi, S. Chen, Ceram. Int. 47 (2021) 28014–28020.
[31] P. Yin, Z. Shi, L. Sun, P. Xie, D. Dastan, K. Sun, R. Fan, Polym. Compos. 42 (2021) 3000–3010.
[32] I. Hotovy, V. Rehacek, P. Siciliano, S. Capone, L. Spiess, Thin Solid Films 418 (2002) 9.
[33] I. Hotovy, J. Huran, P. Siciliano, S. Capone, L. Spiess, V. Rehacek, Sens. Actuators, B 78 (2001) 126.
[34] I. Hotovy, J. Huran, L. Spiess, R. Capkovic, S. Hascík, Vacuum 58 (2000) 300.
[35] C. Imawan, F. Solzbacher, F. Steffes, E. Obermeier, Sens. Actuators, B 68 (2000) 184.
[36] N. Brilis, C. Foukaraki, E. Bourithis, D. Tsamakis, A. Giannoudakos, M. Kompitsas, T. Xenidou, A. Boudouvis, Thin Solid Films 515 (2007) 8484.
[37] C. Luyo, R. Ionescu, L.F. Reyes, Z. Topalian, W. Estrada, E. Llobet, C.G. Granqvist, P. Heszler, Sensor. Actuator. B 138 (2009) 14.
[38] S. Kailasa Ganapathi, M. Kaur, R. Singh, V.I. Singh, A.K. Debnath, K.P. Muthe, S. C. Gadkari, ACS Appl. Nano Mater. 2 (2019) 6726.
[39] X. Yin, W. Zhou, D. Dastan, J. Li, X. Tan, Y. Liu, X. Gao, X. Ma, Mater. Sci. Semicond. Process. 149 (2022), 106883.
[40] X. Yin, S. Wu, D. Dastan, S. Nie, Y. Liu, Z. Li, Y. Zhou, J. Li, A. Faik, K. Shan, Z. Shi, M. Abbasi Tarighat, X. Ma, Surface. Interfac. 25 (2021), 101190.
[41] P. Ravikumar, D. Taparia, P. Alagarsamy, J. Supercond, Magn 31 (2018) 3761. Nov.
[42] Xi-Tao Yin, Li Jing, Qi Wang, Davoud Dastan, Zhi-Cheng Shi, Najlaa Alharbi, Hamid Garmestani, Xiao-Ming Tan, Ying Liu, Xiao-Guang Ma, Langmuir 37 (46) (2021) 13548–13558.
[43] M. Paidar, V.V. Ramalingam, A. Moharrami, O.O. Ojo, A. Jafari, S. Sadreddini, Vacuum 1092 (2020) 98.
[44] A. Jafari, M. Mosavat, A. Meidanchi, H. Hossienkhani, J. Chem. Res. 42 (2018) 73.
[45] A. Jafari, M. Ghoranneviss, A.S. Elahi, J. Inorg. Organomet. Polym. Mater. 26 (2016) 254.
[46] L.D.L.S. Valladares, A. Ionescu, S. Holmes, C.H.W. Barnes, A.B. Domínguez, et al., J. Vac. Sci. Technol. 32 (2014), 051808.
[47] M.R. Pinnel, H.G. Tompkins, D.E. Heath, J. Electrochem. Soc. 126 (1979) 1274.
[48] P. Mohanty, C. Rath, P. Mallick, R. Biswal, N.C. Mishra, Physica B 405 (2010) 711.
[49] A. Jafari, R. Alipour, M. Ghoranneviss, Bull. Mater. Sci. 38 (2015) 707.
[50] A. Jafari, Z. Ghoranneviss, A.S. Elahi, M. Ghoranneviss, N.F. Yazdi, A. Rezaei, Adv. Mech. Eng. 6 (2014), 373847.
[51] K.O. Ukoba, A.C. Eloka-Eboka, F.L. Inambao, Sustainable Energy Reviews 82 (2018 Renewable) 2900.
[52] J. Saju, O.N. Balasundaram, Materials Science-Poland 37 (2019) 3.
[53] R. Barir, B. Benhaoua, S. Benhamida, R. Rahal, T. Sahraoui, R. Gheriani, J. Nanomater. 1 (2017).
[54] H. Hajakbari, J. Nanostructure. Chem 10 (2020) 97.
[55] K. Shan, Z. Yi, X. Yin, D. Dastan, F. Altaf, H. Garmestani, F. Alamgir, Surface. Interfac. 21 (2020), 100762.
[56] M.A. Chakhoum, A. Boukhachemb, M. Ghamnia, N. Benameur, N. Mahdhi, K. Raouadi, M. Amlouk, Spectrochim. Acta Mol. Biomol. Spectrosc. 205 (2018) 649–660.
[57] E.F. Funkenbusch, B.C. Cornilsen, Solid State Commun. 40 (1981) 707.
[58] Y. Tian, L. Gong, X. Qi, Y. Yang, X. Zhao, Coatings 9 (2019) 634.
[59] A. Loukil, A. Boukhachem, M. Ben Amor, M. Ghamnia, K. Raouadi, Ceram. Int. 42 (2016) 8274–8289.
[60] R.E. Dietz, G.I. Parisot, A.E. Meixner, Phys. Rev. B 4 (1991) 2302.
[61] D.Y. Jiang, J.M. Qin, X. Wang, S. Gao, Q.C. Liang, J.X. Zhao, Vacuum 86 (2012) 1083.
[62] D.A. Wruck, M. Rubin, J. Electrochem. Soc. 140 (1993) 1097.
[63] M. Budde, C. Tschammer, P. Franz, J. Feldl, M. Ramsteiner, R. Goldhahn, M. Feneberg, Oprea A. BarsanN, O. Bierwagen, J. Appl. Phys. 123 (2018), 195301.
[64] N. Mironova-Ulmane, A. Kuzmin, I. Steins, J. Grabis, J. Phys. (Paris): Confer Ser 93 (2007), 012039.
[65] R. Kumar, C. Baratto, G. Faglia, G. Sberveglieri, E. Bontempi, L. Borgese, Thin Solid Films 583 (2015) 233.
[66] T. Yu, X.L. Cheng, X. Zhang, L. Sui, Y. Xu, S. Gao, H. Zhao, L. Huo, J. Mater. Chem. 3 (2015), 11991.
[67] V.D. Kapse, S.A. Ghosh, G.N. Chaudhari, F.C. Raghuwanshi, D.D. Gulwade, Vacuum 83 (2009) 346.
[68] H. Kim, C. Jin, S. Park, S. Kim, C. Lee, Sensor. Actuator. B Chem. 161 (2012) 594.
[69] Z. Qu, Y. Fu, B. Yu, P. Deng, L. Xing, X. Xue, Sensor. Actuator. B Chem. 222 (2016) 78.
[70] P. Rai, Ji-W. Yoon, H.M. Jeong, S.J. Hwang, C.H. Kwak, J.H. Lee, Nanoscale 6 (2014) 8292−−8299.
[71] F. Li, Y. Chen, J. Ma, RSC Adv. 4 (2014) 14201–14205.
[72] S. Poongodi, P.S. Kumar, D. Mangalaraj, N. Ponpandian, P. Meena, Y. Masuda, C. Lee, J. Alloys Compd. 719 (2017) 71–81.
[73] G. Jain, L. Patil, M. Wagh, D. Patil, S. Patil, D. Amalnerkar, Sensor. Actuator. B Chem. 117 (2006) 159–165.
[74] K.S. Yoo, S.D. Han, H.G. Moon, S.-J. Yoon, C.-Y. Kang, Sensors 15 (2015) 15468–15477.
[75] N. Joshi, V. Saxena, A. Singh, S. Koiry, A. Debnath, M.M. Chehimi, D. Aswal, S. Gupta, Sensor. Actuator. B Chem. 200 (2014) 227–234.
[76] C. Liu, K. Hayashi, K. Toko, Sensor. Actuator. B Chem. 161 (2012) 504–509.